ACS Catalysis

pubs.acs.org/acscatalysis Research Article

Unraveling the Mechanism of Ammonia Selective Catalytic Oxidation on Ag/Al_2O_3 Catalysts by Operando Spectroscopy

Guangyan Xu, Yu Zhang, Jingguo Lin, Yibao Wang, Xiaoyan Shi, Yunbo Yu, and Hong He*

Cite This: *ACS Catal.* 2021, 11, 5506−5516 Read Online

ABSTRACT: Ammonia leakage from the aftertreatment of diesel vehicles arouses serious environmental concerns, thus demanding a high-efficiency ammonia elimination catalyst. In the present work, the mechanism of ammonia selective catalytic oxidation (NH_3-SCO) on Ag/Al_2O_3 catalysts was investigated by operando spectroscopy (DRIFTS-MS and DR-UV−vis). Characterization results show that silver cations are predominant on Ag/Al_2O_3 samples with a low silver loading, whereas many silver nanoparticles are present on 10 wt % Ag/Al_2O_3. Operando DR-UV−vis analysis confirms that silver nanoparticles are the active sites for NH_3 oxidation, while silver cations are inert in this reaction. During NH_3 oxidation, oxygen activation on the silver nanoparticles induces the oxidation of metallic silver, whereas NH_3 dehydrogenation, in turn, reduces the oxidized silver species. Notably, the NH_3-SCO reaction on 10 wt % Ag/Al_2O_3 could be divided into three regions: the light-off region, high-efficiency region, and high-temperature region. The reaction pathway of NH_3 oxidation is nearly related to oxygen activation on the silver nanoparticles; that is, a slow activation rate results in the generation of N_2O, whereas rapid activation induces the quick dehydrogenation of NH_3 to produce NO. Instead, appropriate rates for O_2 activation and NH_3 dehydrogenation are essential for N_2 formation during NH_3 oxidation.

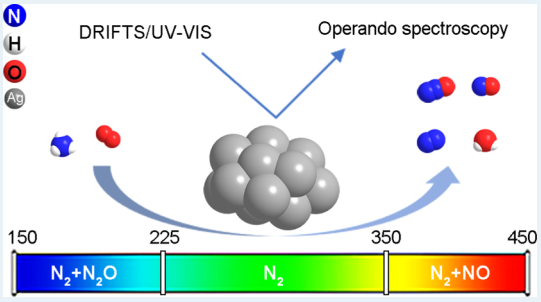

KEYWORDS: *ammonia, selective catalytic oxidation, Ag/Al_2O_3, operando DRIFTS-MS, operando DR-UV−vis*

1. INTRODUCTION

Ammonia (NH_3) plays an essential role in industrial nitrogen chemistry, while its emission poses a great challenge to environmental protection.[1] In particular, ammonia is widely used as a reductant for the selective catalytic reduction (NH_3-SCR) of nitric oxides (NO*x*) emitted from heavy-duty diesel vehicles.[2] However, NH_3 leakage in aftertreatment systems has gradually increased due to the increase in urea injection to meet stricter NO*x* emission regulations.[3] As a result, NH_3 leakage has recently been regulated in the new diesel vehicle emission regulations. There are several techniques for NH_3 abatement, including absorption, adsorption, catalytic combustion, catalytic decomposition, and thermal catalytic oxidation.[4] Among these, selective catalytic oxidation of NH_3 (NH_3-SCO) to N_2 and H_2O is an efficient technology for NH_3 abatement in diesel vehicles.[5]

The NH_3-SCO technique for diesel vehicles needs to completely oxidize NH_3 to yield harmless N_2 and H_2O at a low temperature below 300 °C without the regeneration of undesirable NO*x*. Until now, three types of materials have been investigated in the NH_3-SCO reaction: (i) noble metal-based catalysts (Pt, Pd, Rh, Ir, Ru, Au, and Ag),[6−13] (ii) transition metal oxide-based catalysts (CuO, Fe_3O_4, Co_3O_4, NiO, and V_2O_5),[14−19] and (iii) modified zeolite catalysts (ZSM-5, mordenite, Y, and β).[20−24] Noble metal-based catalysts possess high efficiency for NH_3 oxidation at low temperatures below 300 °C, whereas they suffer from poor N_2 selectivity and high cost.[5] Although transition metal oxide-based catalysts and modified zeolite catalysts show better N_2 selectivity in the NH_3-SCO reaction, they are insufficient for NH_3 oxidation at low temperatures. In contrast, alumina-supported silver (Ag/Al_2O_3) has proven to be a suitable NH_3 abatement catalyst due to its excellent low-temperature activity, N_2 selectivity, and low cost compared with other noble metals.[25−28]

There remain some debates on the mechanism and active sites of NH_3-SCO over Ag/Al_2O_3, which hinder the design and improvement of silver catalysts from meeting the stricter regulation on ammonia leakage. Hitherto, three mechanisms have been proposed for the NH_3-SCO reaction: (i) the imide mechanism, in which imide (−NH) and nitrosyl (HNO) intermediates are produced,[29−31] (ii) the hydrazine mechanism, involving hydrazine (N_2H_4) as an intermediate,[18,32−34] and (iii) the internal selective catalytic reduction mechanism (i-SCR) that contains two steps of NH_3 oxidation to yield

Received: March 6, 2021
Revised: April 8, 2021

NOx and NH_3-SCR.[11,17,23,24,32,35,36] Gang et al.[25,26] proposed that NH_3 oxidation over supported silver catalysts obeyed the i-SCR mechanism and that the low-temperature activity was dependent on the dissociative or nondissociative adsorption of O_2. Zhang et al.[27,28] suggested that NH_3-SCO over Ag/Al_2O_3 catalysts obeyed the imide mechanism at low temperatures below 140 °C, while following the i-SCR mechanism at high temperatures above 140 °C. Recently, Wang et al.[37,38] proposed a "N_2^- mechanism" for NH_3 oxidation over nanosized Ag/Al_2O_3 catalysts in which NH_3 is dehydrogenated to form amide and imide, followed by the formation of N_2^- species as well as gaseous N_2. Despite extensive research, there remains a debate on the elementary reaction steps and the active sites in the NH_3-SCO reaction over Ag/Al_2O_3 catalysts. One of the crucial reasons is that the previous works usually investigated the reaction mechanism by ex situ technologies, which made drawing definite conclusions about the active sites and reaction mechanism of NH_3-SCO difficult.

The above problems highlight the importance of operando technologies to investigate catalysts and reaction mechanisms under realistic working conditions.[9,39] In the present work, high-efficiency Ag/Al_2O_3 catalysts were synthesized and characterized by Brunauer−Emmett−Teller (BET), X-ray diffraction (XRD), X-ray photoelectron spectroscopy (XPS), ultraviolet−visible (UV−vis) spectrophotometry, and high-resolution transmission electron microscopy (HR-TEM). Besides, the reaction mechanism of NH_3 oxidation on Ag/Al_2O_3 catalysts was investigated by operando diffuse reflectance infrared Fourier transform spectroscopy combined with mass spectrometry (DRIFTS-MS) and diffuse reflectance UV−vis (DR-UV−vis) spectrophotometry. This study provides deep insights into the reaction mechanism of NH_3-SCO and offers some advice for the design of high-efficiency NH_3-SCO catalysts.

2. EXPERIMENTAL SECTION

Ag/Al_2O_3 catalysts with 1 and 10 wt % silver loadings were prepared using an impregnation method.[40,41] Boehmite (SASOL, SB1) was added into deionized water with stirring to form a suspension. Silver nitrate (AR) was dissolved in deionized water and then added into the above suspension with stirring. Afterward, the excess water was evaporated, and the samples were dried in an oven at 100 °C for 12 h. Finally, these samples were calcined in a muffle furnace at 600 °C for 3 h. Al_2O_3 was prepared by the same procedure without impregnating with silver nitrate.

BET analysis was performed on a physical adsorption instrument (Micromeritics, ASAP 2020).[42] XRD measurement was carried out on a D8-ADVANCE (Bruker) diffractometer using Cu Kα radiation (40 kV, 40 mA). XPS analysis was performed on an X-ray photoelectron spectrometer (AXIS Supra, Kratos Analytical Ltd.). The spectra were collected at a step size of 0.10 eV, using C 1s (284.8 eV) for calibration. H_2 temperature-programmed reduction (H_2-TPR) was performed on a Micromeritics AutoChem 2920 II chemisorption analyzer.[41] The sample (50 mg) was pretreated in 10% O_2/He at 300 °C for 30 min and cooled down to 20 °C in Ar, followed by TPR in 10% H_2/Ar (50 mL/min) at a rate of 10 °C/min. UV−vis analysis was conducted on a UV−vis spectrophotometer (LAMBDA 650, PerkinElmer).[40] The spectra were recorded at a resolution of 1 nm using Al_2O_3 as the reference. The catalyst's morphology was investigated by a high-resolution transmission electron microscope (2100 Plus, JEOL).

The catalytic tests were conducted in a fixed-bed reactor (i.d. 7 mm).[40,43] The gas composition was composed of 500 ppm NH_3, 5% O_2, 5% H_2O (when added), and 5% CO_2 (when added) in N_2 balance (500 mL/min). A 200 mg sample (40−60 mesh) was employed, corresponding to a gas hourly space velocity of 110,000 h^{-1}. The reactants and products (NH_3, N_2O, and NO) were monitored by a Fourier transform infrared (FT-IR) spectrometer (Nicolet iS 10). The formation of NO_2 was negligible (<3 ppm). The NH_3 conversion and N_2 formation were calculated according to eqs 1 and 2, respectively.

$$\text{NH}_3\ \text{conversion}\ (\%) = \frac{[\text{NH}_3]_{\text{in}} - [\text{NH}_3]_{\text{out}}}{[\text{NH}_3]_{\text{in}}} \times 100\% \tag{1}$$

$$\text{N}_2\ \text{formation (ppm)} = \frac{[\text{NH}_3]_{\text{in}} - [\text{NH}_3]_{\text{out}} - 2 \times [\text{N}_2\text{O}] - [\text{NO}]}{2} \tag{2}$$

Kinetic studies were conducted in the above reactor. The NH_3 conversion was controlled below 30% via varying the weight of the sample. Internal and external diffusion effects had been eliminated according to our previous works.[37,40] The concentrations of NH_3 and O_2 were varied from 100 to 600 ppm and from 1 to 10%, respectively. Turnover frequency was calculated according to eq 3, where F_{NH_3}, X_{NH_3}, W, L, and M_{Ag} represent the flow rate (mol/s), NH_3 conversion (%), the sample weight (g), silver loading (%), and silver molar mass (g/mol), respectively. D_{Ag} represents silver dispersion, which was calculated according to D_{Ag} (%) = 1.34/d (nm) by assuming that the silver species were present as spherical crystallites, whereas d is the average silver particle size obtained from the HR-TEM images[44]

$$\text{TOF}\ (\text{s}^{-1}) = \frac{F_{\text{NH}_3} \times X_{\text{NH}_3}}{W \times L \times D_{\text{Ag}} \div M_{\text{Ag}}} \tag{3}$$

Operando DRIFTS-MS experiments were performed by FT-IR spectroscopy (Nicolet iS 50) and online MS (InProcess Instruments, GAM 200).[41,45] A powder sample (~60 mg) was placed into a Harrick Scientific cell. The typical gas composition was composed of 500 ppm NH_3 and 5% O_2 in Ar balance (100 mL/min, 75,000 h^{-1}). The spectra were recorded with an accumulation of 100 scans (4 cm^{-1}) and represented in Kubelka−Munk units. The products, including N_2, N_2O, NO, and H_2O, were monitored by online MS. Before each experiment, the sample was pretreated in 5% O_2/Ar at 450 °C for 1 h.

Operando DR-UV−vis experiments were conducted on the above UV−vis spectrophotometer equipped with a Harrick Scientific cell. Except for using N_2 balance, the settings for operando DR-UV−vis experiments were the same as those for the operando DRIFTS experiments. The spectra were collected from 800 to 200 nm at a rate of 1 nm/s with 5 nm resolution and represented in Kubelka−Munk units. The DR-UV−vis data were obtained by continuously measuring the absorbance at 450 nm at 1 point/s time resolution.

https://doi.org/10.1021/acscatal.1c01054
ACS Catal. 2021, 11, 5506−5516

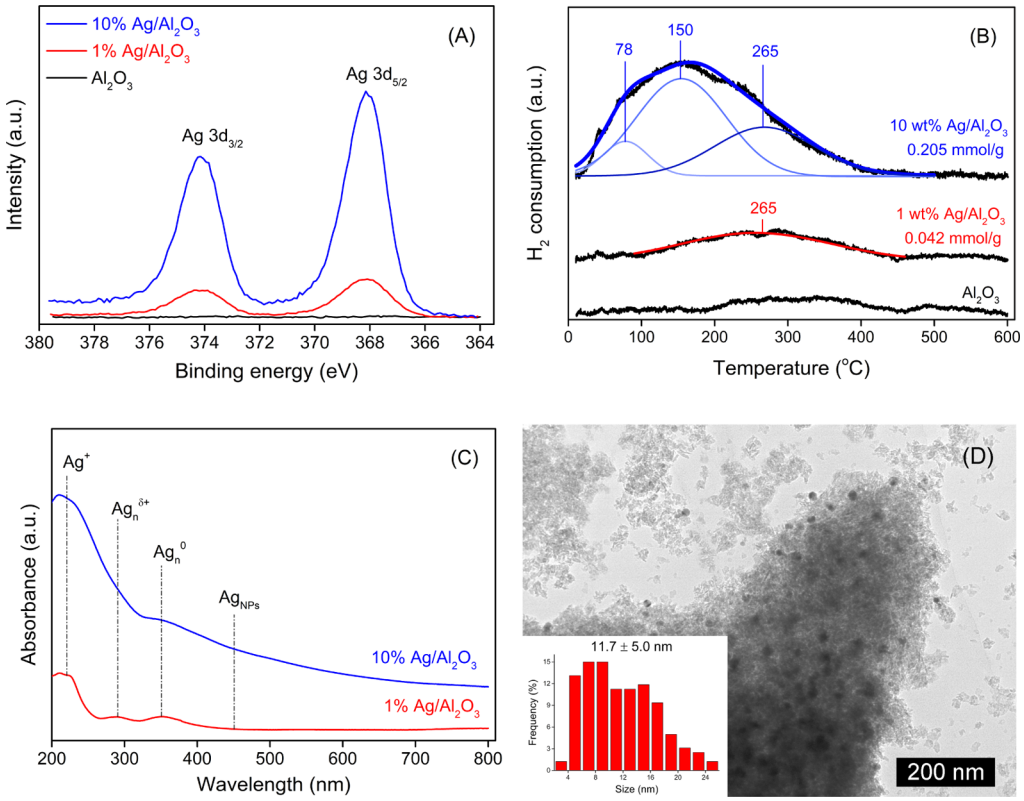

Figure 1. XPS spectra (A), H_2-TPR profiles (B), and UV−vis spectra (C) of Ag/Al_2O_3 catalysts and HR-TEM image of 10 wt % Ag/Al_2O_3 (D).

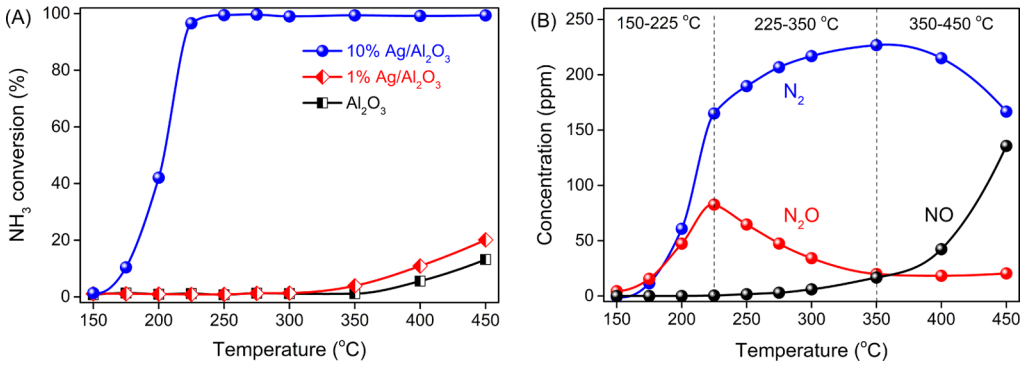

Figure 2. NH_3 conversion on Ag/Al_2O_3 catalysts in NH_3-SCO (A) and product concentrations on 10 wt % Ag/Al_2O_3 (B).

3. RESULTS

3.1. Characterization. Various techniques were employed to investigate the surface and structural properties of the Ag/Al_2O_3 catalysts (Figure 1). The XRD patterns showed that only the γ-Al_2O_3 crystal phase was observed for the Al_2O_3 and Ag/Al_2O_3 samples (Figure S1).[42] In contrast, no silver phase was observed on the Ag/Al_2O_3 samples, indicating the good dispersion or amorphous nature of the silver species.[27] Pure Al_2O_3 had a specific surface area of 203.3 m^2/g, while the impregnation of silver species did not significantly affect the surface and pore structure of Ag/Al_2O_3 samples (Table S1). The slight increase in the specific surface area of 1 wt % Ag/Al_2O_3 (225.4 m^2/g) might be due to the influence of silver species on the pore structure of the Al_2O_3 support, which has also been observed in a previous work.[43] XPS analysis showed that the surface concentrations of silver species on the 1 wt % Ag/Al_2O_3 and 10 wt % Ag/Al_2O_3 were 2.36 and 12.5%, respectively, which were only slightly higher than the overall silver contents (Figure 1A). H_2-TPR analysis showed that 1 wt % Ag/Al_2O_3 had a single H_2 consumption peak (~265 °C), attributed to the reduction of dispersed Ag^+ cations (Figure 1B).[41] The H_2 consumption on this sample was 0.042 mmol/g, which is approximately equal to the theoretical value of 0.046 mmol/g (Ag/H_2 = 1:2), indicating that the silver species were mainly present in the oxidized state. Instead, there were three peaks observed on 10 wt % Ag/Al_2O_3, attributed to the reduction of surface oxygen on Ag (78 °C), Ag_2O nanoparticles (150 °C), and dispersed Ag^+ cations (265 °C).[26,37] The H_2 consumption on the 10 wt % Ag/Al_2O_3 was 0.205 mmol/g, which is significantly lower than the theoretical value (0.46 mmol/g), indicating that a certain amount of silver species was in the metallic state and could not be reduced by H_2.

In order to eliminate the interference by Al_2O_3 absorbance, the Al_2O_3 UV−vis spectrum was subtracted from the spectra of the Ag/Al_2O_3 catalysts (Figure 1C). Four absorbance peaks

https://doi.org/10.1021/acscatal.1c01054
ACS Catal. 2021, 11, 5506−5516

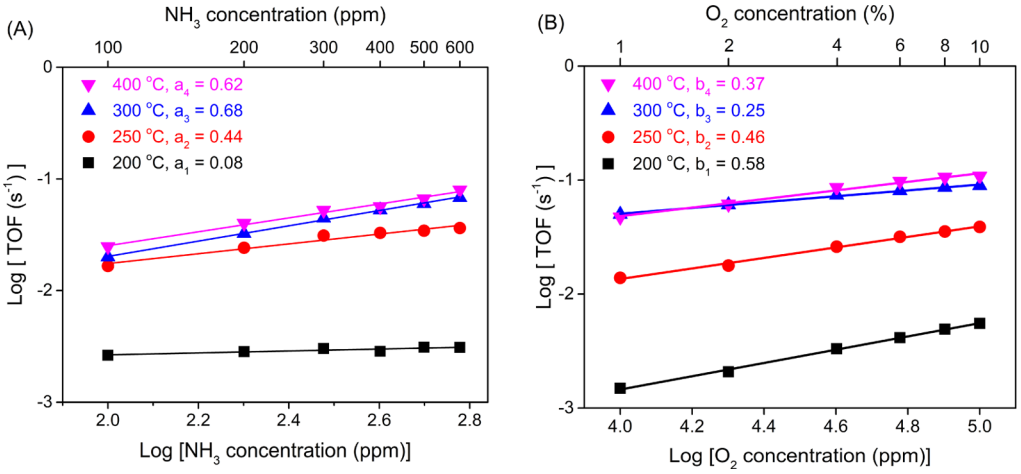

Figure 3. Reaction rate of NH_3 conversion as a function of NH_3 (A) and O_2 (B) concentrations over 10 wt % Ag/Al_2O_3 at different temperatures. Typical feed composition: 500 ppm NH_3 and 5% O_2 in N_2 balance.

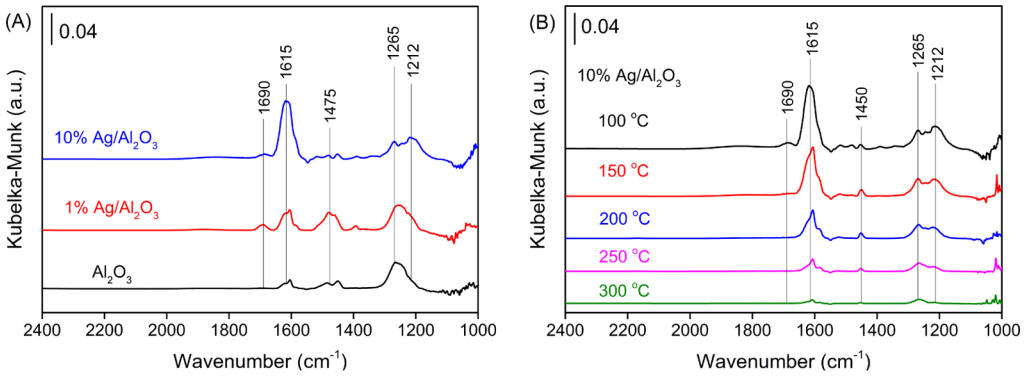

Figure 4. NH_3 adsorption on Al_2O_3 and Ag/Al_2O_3 catalysts at 100 °C (A) and 10 wt % Ag/Al_2O_3 at different temperatures (B).

were observed for the Ag/Al_2O_3 samples and were attributed to the dispersed silver cations (220 nm), partially oxidized silver clusters (290 nm), metallic silver clusters (350 nm), and metallic silver nanoparticles (450 nm).[27,46−48] On Ag/Al_2O_3 with a low silver loading (1 wt %), dispersed silver cations dominated the surface and accounted for about 70% of the total silver species, accompanied by a small amount of silver clusters. Instead, in addition to silver cations, there were a large number of silver clusters and nanoparticles present on 10 wt % Ag/Al_2O_3, resulting in a strong absorption in the visible light region. HR-TEM images further confirmed that silver nanoparticles with an average diameter of 11.7 nm were present on the 10 wt % Ag/Al_2O_3 catalyst, whereas silver cations were hardly observed due to the limitations of the HR-TEM analysis (Figures 1D and S2).

3.2. Catalytic Activity. As shown in Figure 2, Al_2O_3 was entirely inactive for NH_3 oxidation with a maximum conversion of 10% at 450 °C, while impregnation with a low silver content hardly improved the catalytic performance of 1 wt % Ag/Al_2O_3. In contrast, the 10 wt % Ag/Al_2O_3 catalyst exhibited a high efficiency for NH_3 oxidation, with 96.6% NH_3 conversion at 225 °C. Notably, the NH_3-SCO reaction over 10 wt % Ag/Al_2O_3 could be divided into three reaction regions, consistent with a similar phenomenon observed in NH_3 oxidation on Pd/Al_2O_3 catalysts.[9] In the light-off region (150−225 °C), NH_3 oxidation started occurring, and the formation of N_2 and N_2O was rapidly increased as the temperature rose; in the high-efficiency region (225−350 °C), the generation of N_2 was highly efficient and increased gradually, accompanied by a gradual decline in N_2O production; in the high-temperature region (350−450 °C), NO formation gradually increased at the expense of decreased N_2 generation. Moreover, the heating/cooling cycle test with the coexistence of CO_2 and H_2O shows that the stability of the Ag/Al_2O_3 catalysts should be further improved (Figure S3).

To further investigate the kinetics of NH_3-SCO over 10 wt % Ag/Al_2O_3, the conversion rate of NH_3 as a function of NH_3 and O_2 concentrations was measured at different temperatures (Figure 3). In the light-off region (200 °C), the reaction order of NH_3 was 0.08, indicating that NH_3 adsorbed on the catalyst surface before its further reaction. In the high-efficiency region, however, the reaction order of NH_3 gradually increased to 0.44 and 0.68 at 250 and 300 °C, respectively. In contrast, the reaction order of O_2 gradually decreased from 0.58 to 0.46 and 0.25 as the temperature increased from 200 to 250 and 300 °C, respectively, revealing that more gaseous O_2 was activated on the catalyst surface to participate in the reaction. In the high-temperature region (400 °C), the reaction order of NH_3 remained stable (0.62), whereas the order of O_2 increased to 0.37 instead. Moreover, increasing the reaction temperature from 200 to 300 °C significantly increased the reaction rate of NH_3 oxidation, whereas a further increase to 400 °C did not further enhance the NH_3 conversion. By the way, changes in NH_3 and O_2 concentrations only slightly affected the N_2 selectivity in the kinetic study (not shown).

https://doi.org/10.1021/acscatal.1c01054
ACS Catal. 2021, 11, 5506−5516

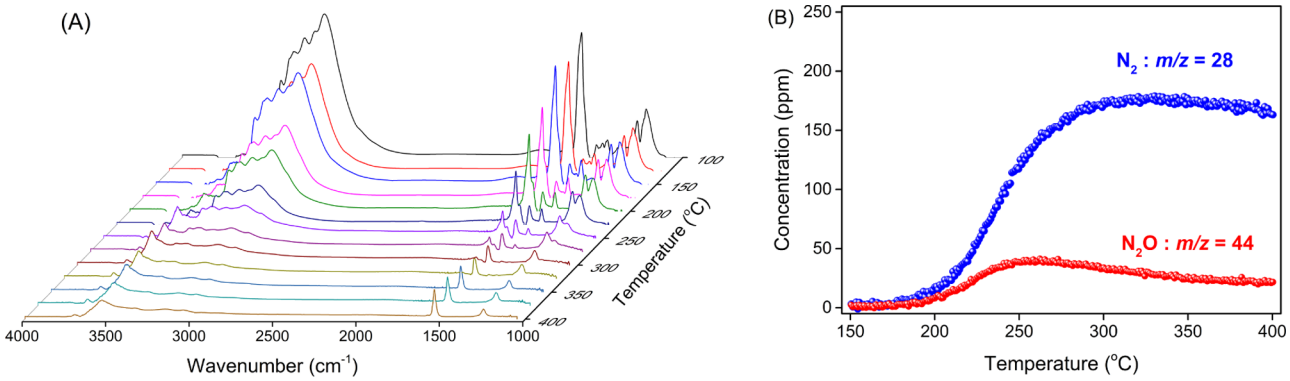

Figure 5. TPSR experiment of NH_3-SCO reaction on 10 wt % Ag/Al_2O_3: surface intermediates (A) and gaseous products (B). Feed composition: 500 ppm NH_3 and 5% O_2 in Ar balance.

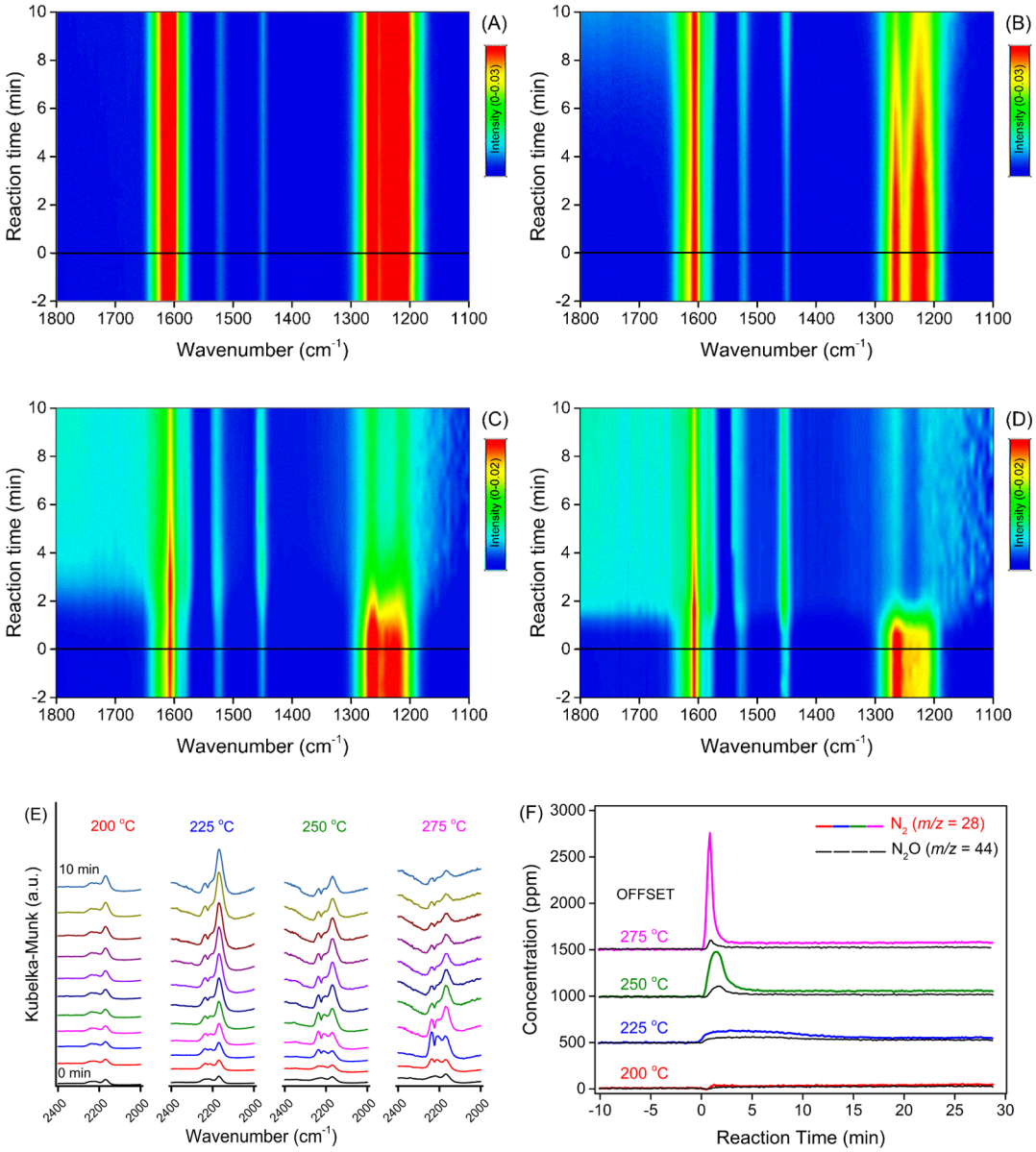

Figure 6. Reactivity of adsorbed NH_3 species toward O_2 over 10 wt % Ag/Al_2O_3 at 200 (A), 225 (B), 250 (C), and 275 °C (D) and the surface intermediates (E) and gaseous products (F) at different temperatures. The 10 wt % Ag/Al_2O_3 catalyst was pre-exposed to NH_3 for 60 min and then exposed to NH_3 + O_2 for 30 min. Feed composition: 500 ppm NH_3 and 5% O_2 in Ar balance.

https://doi.org/10.1021/acscatal.1c01054
ACS Catal. 2021, 11, 5506−5516

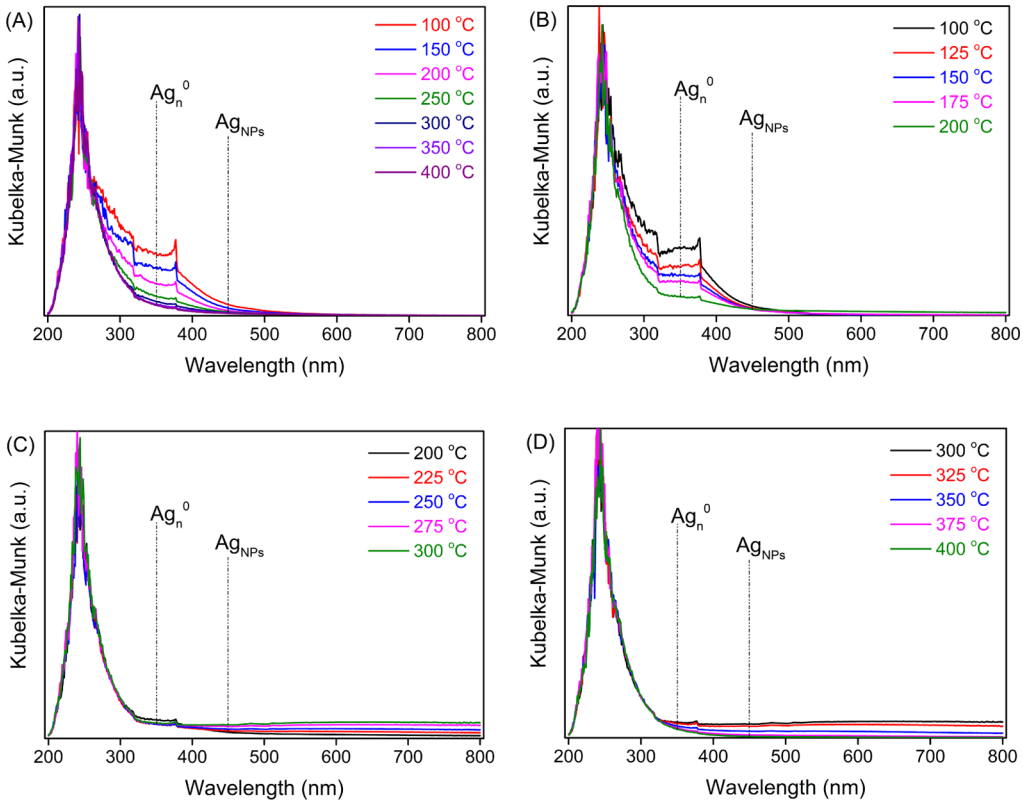

Figure 7. Operando DR-UV−vis spectra of 10 wt % Ag/Al_2O_3 in a flow of O_2/N_2 (A) and $NH_3/O_2/N_2$ (B−D) at different temperatures. Feed composition: 500 ppm NH_3 and 5% O_2 in N_2 balance.

3.3. Operando DRIFTS-MS Experiments. Operando DRIFTS-MS experiments were conducted to investigate the surface intermediates and gaseous products in NH_3 oxidation over Ag/Al_2O_3 catalysts. Figure 4 shows the DRIFTS spectra of NH_3 adsorption on the Al_2O_3 and Ag/Al_2O_3 catalysts at different temperatures. Several peaks were observed on Al_2O_3, which were attributed to NH_3 adsorbed on different acid sites. Specially, the band at 1615 cm^{-1} was attributed to the asymmetric stretch of NH_3 adsorbed on Lewis acid sites, while the peaks at 1265 and 1212 cm^{-1} were assigned to the symmetric stretch of the above adsorbed NH_3. Instead, the peaks at 1690 and 1475 cm^{-1} were due to the asymmetric and symmetric deformation modes of NH_3 coordinated on Brønsted acid sites, respectively.[28,49] Impregnation with a small amount of silver species slightly increased the number of Brønsted acid sites on 1 wt % Ag/Al_2O_3, possibly due to the formation of hydroxyl groups connected to the dispersed silver cations. By contrast, the Brønsted acid sites vanished on 10 wt % Ag/Al_2O_3, accompanied by a significant increase in the Lewis acid sites. It was speculated that high-density silver species covered the surface of Al_2O_3, and the metallic silver nanoparticles served as new Lewis acid sites for NH_3 adsorption. NH_3 adsorbed on the Lewis acid sites on 10 wt % Ag/Al_2O_3 was gradually desorbed as the temperature rose above 200 °C (Figure 4B), whereas it was less temperature-sensitive on the Al_2O_3 catalyst (Figure S4).

A temperature-programmed surface reaction (TPSR) experiment for the NH_3-SCO reaction was conducted on 10 wt % Ag/Al_2O_3 while increasing the temperature from 100 to 450 °C at a rate of 2 °C/min (Figure 5). Before ramping up, the sample was exposed to NH_3/O_2 at 100 °C for 90 min to reach a stable state. At 100 °C, a large amount of NH_3 adsorbed on the Lewis acid sites, whereas the formation of N_2 and N_2O was negligible (not shown). As the temperature increased from 150 to 250 °C, the amount of adsorbed NH_3 gradually decreased, accompanied by the rapid formation of N_2 and N_2O. Meanwhile, two weak peaks at 2237 and 2210 cm^{-1} were observed (Figure S5) and were attributed to the adsorption of N_2O (Figure S6). In addition, a new peak at 2170 cm^{-1} was found, which has rarely been reported on Ag/Al_2O_3 catalysts in previous literature. As this peak gradually strengthened as the temperature increased from 175 to 225 °C, which was consistent with the light-off of NH_3 oxidation, it should be due to the intermediates of NH_3 oxidation. Recently, a similar peak was also observed on the supported Pd catalysts during NH_3 oxidation and was assigned to the asymmetric stretch of dinitrogen species originating from the dissociative adsorption of NH_3.[9] Hence, the band at 2170 cm^{-1} was attributed to the N═N stretch of dinitrogen species (possibly NH═NH species), which served as the precursor for the formation of N_2 and N_2O.

As the temperature further rose from 250 to 350 °C, NH_3 adsorption rapidly decreased, accompanied by the gradual formation of nitrates (1545 and 1250 cm^{-1}).[28] At the same time, N_2 production continuously increased and remained at a high level, whereas N_2O formation gradually decreased. In the high-temperature region (above 350 °C), only nitrate species were observed on the catalyst surface, and the N_2 generation slightly decreased as the temperature further rose. At 400 °C, the removal of NH_3 from the reaction gas ($NH_3 + O_2$) did not affect nitrate adsorption, indicating that nitrates were inert species in this reaction (Figure S7). Because sufficient NO could be formed only at temperatures above 400 °C (Figure 2), MS did not detect the generation of NO in the TPSR

https://doi.org/10.1021/acscatal.1c01054
ACS Catal. 2021, 11, 5506−5516

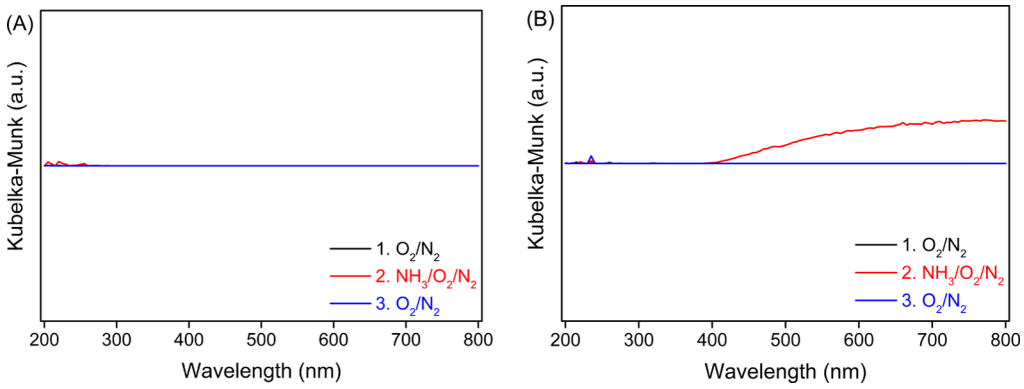

Figure 8. Operando DR-UV−vis spectra of 1 wt % Ag/Al_2O_3 (A) and 10 wt % Ag/Al_2O_3 (B) under different conditions at 300 °C. Feed composition: 500 ppm NH_3 and 5% O_2 in N_2 balance.

experiment. The slightly higher light-off temperature (about 33 °C) for NH_3 conversion in the DRIFTS-MS experiment compared to the catalytic test (Figure 2) could be attributed to the differences in the experimental systems.

Moreover, the reactivity of adsorbed NH_3 was measured on the 10 wt % Ag/Al_2O_3 catalyst at different temperatures (Figure 6). At 200 °C, the adsorbed NH_3 species hardly reacted with O_2 to form the surface intermediate (2170 cm^{-1}), not to mention the gaseous products of N_2 and N_2O. This indicated that O_2 activation and NH_3 dehydrogenation to form dinitrogen species were the limiting steps at this temperature. Incidentally, the formation of trace amounts of dinitrogen species and adsorbed N_2O during NH_3 adsorption could be due to the reaction between the adsorbed NH_3 species and chemisorbed oxygen species on the Ag/Al_2O_3 surface. At 225 °C, NH_3 adsorbed on the Lewis acid sites (1615, 1264, and 1212 cm^{-1}) gradually reacted with gaseous O_2 to produce dinitrogen species and adsorbed N_2O, accompanied by the formation of gaseous N_2 and N_2O. The formation of a high amount of dinitrogen species and a low concentration of gaseous N_2 revealed that further reaction of dinitrogen species to produce N_2 might be the limiting step at this temperature. Besides, the peak for molecular H_2O (1600−1650 cm^{-1}) originating from the SCO reaction would interfere with the peak (1615 cm^{-1}) due to the Lewis acid site. As the temperature further rose to 250 °C, notably, the adsorbed NH_3 species' reactivity was remarkably enhanced, and the N_2 generation was more than 450 ppm in the first 3 min. At 275 °C, the adsorbed NH_3 was much more reactive toward gaseous O_2, and the peak for N_2 formation was extraordinarily sharp and intense (∼1200 ppm). Meanwhile, the concentration of surface dinitrogen species was negligible in the steady NH_3-SCO reaction, revealing that its subsequent decomposition was fast at high temperatures. In order to better identify the intermediates of NH_3 oxidation, a spectrum was obtained by subtracting the spectrum in NH_3 from the spectrum in NH_3/O_2 (Figure S8). Two new peaks (1550 and 1455 cm^{-1}) were observed and were attributed to amide ($-NH_2$) and hydrazine (NH_2-NH_2), respectively.[18]

3.4. Operando DR-UV−vis Experiments. In order to study the dynamic change of silver species during the NH_3-SCO reaction, an operando DR-UV−vis experiment was conducted on the 10 wt % Ag/Al_2O_3 catalyst at different temperatures (Figure 7). To eliminate the interference by the support, Al_2O_3 was used as the reference. Incidentally, the differences between the ex situ UV−vis spectra and operando DR-UV−vis spectra could be attributed to the different experimental modes. In the flow of O_2/N_2 (Figure 7A), as the temperature gradually increased from 100 to 400 °C (2 °C/min), the number of metallic silver clusters (350 nm) and metallic silver nanoparticles (450 nm) gradually decreased, indicating that metallic silver was gradually oxidized at high temperature. Instead, during the TPSR experiment of NH_3-SCO reaction, the metallic silver species exhibited different characteristics with the rising temperature. As the temperature increased from 100 to 200 °C (Figure 7B), the amount of metallic silver species gradually decreased, consistent with that observed in the absence of NH_3. When the temperature further rose to 300 °C (Figure 7C), it should be highlighted that a broad absorbance appeared in the visible region (400−800 nm) and gradually strengthened, which could be attributed to the surface plasmon absorption of silver nanoparticles.[50] In contrast, the above absorbance gradually weakened as the temperature further increased from 300 to 400 °C (Figure 7D). The absence of surface plasmon absorption on 10 wt % Ag/Al_2O_3 in O_2/N_2 (Figure 7A) may be due to the adsorption of O_2 on the surface of silver nanoparticles. Therefore, NH_3 significantly changed the valence state of silver species in the NH_3-SCO reaction over the Ag/Al_2O_3 catalyst.

In order to clarify the roles of different silver species in the NH_3-SCO reaction, a step response experiment was conducted on 1 wt % Ag/Al_2O_3 and 10 wt % Ag/Al_2O_3 (Figure 8). Before each experiment, these samples were pretreated in O_2/N_2 at 400 °C for 1 h and then cooled down to 300 °C to collect a reference spectrum. Afterward, the samples were sequentially exposed to O_2/N_2, $NH_3/O_2/N_2$, and O_2/N_2 for 30 min each. On 1 wt % Ag/Al_2O_3, the gas composition changes hardly affected the silver species' state. In contrast, on 10 wt % Ag/Al_2O_3, the introduction of NH_3 significantly changed the state of silver species, which exhibited intense absorbance in the visible region, whereas this absorbance vanished after the removal of NH_3. Therefore, it was proposed that silver nanoparticles were the active sites for NH_3 oxidation over 10 wt % Ag/Al_2O_3.

Furthermore, a step-response experiment was conducted on the 10 wt % Ag/Al_2O_3 catalyst to investigate the dynamic changes of metallic silver nanoparticles during the NH_3-SCO reaction (Figure 9). The sample was pretreated and set to the desired temperature to measure a reference (absorbance at 450 nm, which refers to the metallic silver nanoparticle). It was then sequentially exposed to $NH_3/O_2/N_2$, O_2/N_2, NH_3/N_2, and O_2/N_2 for 1 h each. At 200 °C, the introduction of NH_3

https://doi.org/10.1021/acscatal.1c01054
ACS Catal. 2021, 11, 5506−5516

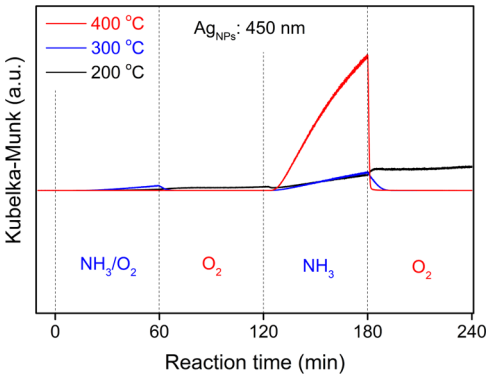

Figure 9. Dynamic change of metallic silver nanoparticles on the 10 wt % Ag/Al_2O_3 catalyst during the switching of the gas composition. Feed composition: 500 ppm NH_3 and 5% O_2 in N_2 balance.

slowly reduced the silver species and increased the number of metallic silver nanoparticles, regardless of the presence of O_2. By contrast, O_2 could not oxidize the above metallic silver nanoparticles even after the removal of NH_3. At the higher temperature of 300 °C, while O_2 could efficiently oxidize the metallic silver nanoparticles, the silver species were still reduced gradually in the presence of NH_3, indicating that the reduction of silver species was faster than their oxidation. As the temperature further rose to 400 °C, the silver species were mainly present in an oxidized state, regardless of the presence of NH_3. At this temperature, NH_3 exhibited a high ability to reduce the silver species, whereas O_2 was a much more potent oxidant. In conclusion, the reduction of silver species was faster than its oxidation at a temperature below 300 °C, while the opposite situation occurred as the temperature further rose to 400 °C.

4. DISCUSSION

As mentioned above, three mechanisms have been proposed for the NH_3-SCO reaction: (i) the imide mechanism (eqs 4−7),[29−31] (ii) the hydrazine mechanism (eqs 8 and 9),[18,32−34] and (iii) the i-SCR mechanism.[10,11,17,23,35] Generally, a consensus has been reached that the NH_3-SCO reaction starts with the adsorption of NH_3, which is further activated by active oxygen species, and then abstracts an H atom to produce amide ($-NH_2$). During this process, the formation of active oxygen species, which originate from the dissociative or nondissociative adsorption of oxygen on the catalyst, is critical for the further activation of NH_3. It was reported that four types of oxygen species could be observed on the Ag/Al_2O_3 catalysts, including adsorbed molecular oxygen, adsorbed atomic oxygen, subsurface oxygen, and bulk dissolved oxygen.[26] Notably, the activation of oxygen is highly dependent on the physical and chemical properties of the active metal on the catalyst.

$$NH_3 + [O] \rightarrow -NH_2 + [OH] \quad (4)$$

$$-NH_2 + [O] \rightarrow -NH + [OH] \quad (5)$$

$$-NH + [O] \rightarrow -HNO \quad (6)$$

$$-HNO + -NH \rightarrow N_2 + H_2O \quad (7)$$

$$-NH_2 + -NH_2 \rightarrow N_2H_4 \quad (8)$$

$$N_2H_4 + O_2 \rightarrow N_2 + 2H_2O \quad (9)$$

UV−vis spectra showed that dispersed silver cations are predominant on 1 wt % Ag/Al_2O_3, whereas many silver nanoparticles are present on 10 wt % Ag/Al_2O_3. Moreover, the HR-TEM images further showed that the above silver nanoparticles had an average diameter of 11.7 nm, while the dispersed silver cations could not be observed due to the limitations of HR-TEM resolution. The absence of peaks of the silver phase in the XRD pattern might be due to the coexistence of metallic and oxidized silver species on 10 wt % Ag/Al_2O_3. More importantly, the operando DR-UV−vis experiment revealed that these metallic silver nanoparticles on 10 wt % Ag/Al_2O_3 gradually converted to oxidized silver nanoparticles as the temperature increased from ambient temperature to high temperature (400 °C). In other words, oxygen was gradually activated on the silver nanoparticles on the 10 wt % Ag/Al_2O_3 catalyst as the temperature rose.

During the NH_3-SCO reaction, neither Al_2O_3 nor 1 wt % Ag/Al_2O_3 was effective for the catalytic oxidation of NH_3, whereas the 10 wt % Ag/Al_2O_3 catalyst exhibited a high efficiency for NH_3 oxidation, with 96.6% conversion at 225 °C. Both Lewis acid sites and Brønsted acid sites exist on Al_2O_3, and impregnation with silver species significantly increases the number of Lewis acid sites on 10 wt % Ag/Al_2O_3, mainly attributed to the metallic silver nanoparticles. Notably, NH_3 adsorbed on these Lewis acid sites exhibited high reactivity toward O_2 to generate N_2 and N_2O (Figure 6). Moreover, the operando DR-UV−vis experiment revealed that silver nanoparticles showed dynamic changes in the NH_3-SCO reaction, whereas the silver cations were completely inactive (Figure 8). Based on the results of operando spectroscopy (DRIFTS-MS and DR-UV−vis), it is proposed that the NH_3-SCO reaction starts with the activation of adsorbed NH_3 by active oxygen species to dehydrogenate to form hydrazine species (NH_2-NH_2). Afterward, the hydrazine species further dehydrogenate to produce NH═NH species, which subsequently react with active oxygen species to yield N_2 and H_2O (eqs 10 and 11). In addition, the NH═NH species could also react with nondissociated $[O_2]$ to generate undesirable N_2O (eq 12).

$$NH_2-NH_2 + [O] \rightarrow NH = NH + H_2O \quad (10)$$

$$NH = NH + [O] \rightarrow N_2 + H_2O \quad (11)$$

$$NH = NH + [O_2] \rightarrow N_2O + H_2O \quad (12)$$

Throughout the above procedures, silver species play an important role in the activation of oxygen, which is critical for the dehydrogenation of adsorbed NH_3. Specifically, oxygen activation on the silver nanoparticles induces the oxidation of metallic silver, whereas the dehydrogenation of adsorbed NH_3 transfers H atoms to the silver nanoparticles and thus reduces the oxidized silver species. The oxidation and reduction rates affect not only the valence state of silver nanoparticles but also the formation of surface intermediates and gaseous products during NH_3 oxidation. It should be highlighted that the NH_3 oxidation over 10 wt % Ag/Al_2O_3 could be divided into three regions: the light-off region where NH_3 oxidation gradually occurred and accelerated to produce both N_2 and N_2O; the high-efficiency region where the N_2 generation was highly efficient and N_2O formation decreased gradually; and the high-temperature region in which NO production gradually increased, accompanied by a slight decrease in N_2 formation.

In the light-off region (150−225 °C), gaseous O_2 was slowly activated on the silver nanoparticles, though the activation

https://doi.org/10.1021/acscatal.1c01054
ACS Catal. 2021, 11, 5506−5516

gradually accelerated as the temperature increased (Figure 7A). As a result, the silver nanoparticles were mainly present in a metallic state at ambient temperature, whereas they were gradually oxidized at elevated temperatures. In this reaction region, it is proposed that both the nondissociative and dissociative adsorbed oxygen species ([O] and [O_2]) coexist on the surface of 10 wt % Ag/Al_2O_3. At a specific temperature (200 °C), the adsorbed NH_3 could be slowly activated and dehydrogenated to reduce the silver nanoparticles, whereas these silver species were hardly reoxidized by O_2 even after the removal of NH_3 (Figure 9). The kinetic study showed that the reaction order of NH_3 at 200 °C was close to zero (0.08), indicating that NH_3 adsorbed on the catalyst surface before its further reaction. Instead, the reaction order of O_2 was 0.58 at 200 °C, revealing that the gaseous O_2 concentration remarkably influenced the reaction rate of NH_3 oxidation. Hence, it is proposed that the reoxidation of silver nanoparticles is the rate-determining step in this reaction region and that the reaction of NH═NH species with [O] and [O_2] is responsible for the generation of N_2 and N_2O (eqs 11 and 12). Compared with other silver-containing catalysts,[26] the 10% Ag/Al_2O_3 catalyst in the present work exhibited lower N_2 selectivity in low temperature regions due to the formation of N_2O.

In the high-efficiency region (225−350 °C), the silver nanoparticles on 10 wt % Ag/Al_2O_3 are mainly present in an oxidized state in O_2/N_2, indicating that O_2 is well activated in this temperature range (Figure 7A). However, during the NH_3-SCO reaction, the reduction of silver nanoparticles by NH_3 is significantly more potent than its further oxidation by O_2, especially at temperatures below 300 °C (Figures 7C and 9). Instead, the oxidation of silver species is remarkably enhanced at temperatures above 300 °C, resulting in the gradual decrease of metallic silver species. The kinetic study showed that the reaction order of NH_3 gradually increased to 0.44 (250 °C) and 0.68 (300 °C), indicating that the adsorption of NH_3 was insufficient, and it also affected the reaction rate. In contrast, the reaction order of O_2 gradually decreased to 0.46 (250 °C) and 0.25 (300 °C), revealing that O_2 was well activated and showed a minor influence on the overall reaction rate. Moreover, the DRIFTS-MS experiment showed that the surface reaction gradually accelerated as the temperature rose and was extremely fast at temperatures above 275 °C. Hence, in this reaction region, the rate-determining step gradually changed from the reoxidation of silver nanoparticles to the adsorption of NH_3 and its further dehydrogenation as temperature increased. Besides, as gaseous O_2 could be rapidly dissociated to produce active [O] species, the formation of N_2O (eq 12) gradually decreased as the temperature rose.

$$-NH + [O] \rightarrow [N] + [OH] \quad (13)$$

$$[N] + [O] \rightarrow [NO] \quad (14)$$

In the high-temperature region (350−450 °C), the silver nanoparticles were present in a completely oxidized state in air. Although NH_3 showed a strong ability to reduce the silver nanoparticles, O_2 exhibited a more potent effect on the oxidation of silver species during the NH_3-SCO reaction. The rapid dehydrogenation of NH_3 possibly resulted in the formation of atomic [N] species, which directly reacted with the abundant [O] species to produce NO (eqs 13 and 14). Therefore, it is crucial to control the dehydrogenation rate of NH_3 to avoid the formation of undesirable NO. While some researchers advised that NO originates from the decomposition of nitrate species, in the present work, however, it was confirmed that nitrate species remain stable on the catalyst surface and serve as spectator species in this reaction (Figure S7). In summary, the reaction pathway of NH_3-SCO over the Ag/Al_2O_3 catalysts is nearly related to the activation of oxygen on the silver nanoparticles, which further governs the subsequent formation of surface intermediates and gaseous products.

5. CONCLUSIONS

The reaction mechanism of NH_3-SCO over Ag/Al_2O_3 was investigated by operando DRIFTS-MS and DR-UV−vis experiments. Dispersed silver cations are predominant on the Ag/Al_2O_3 catalyst with a low silver loading, whereas many silver nanoparticles are present on 10 wt % Ag/Al_2O_3. Silver nanoparticles are the active sites for NH_3 oxidation, while silver cations exhibit little dynamic change during the NH_3-SCO reaction. During NH_3 oxidation, oxygen activation on the silver nanoparticles induces the oxidation of metallic silver, whereas NH_3 dehydrogenation transfers H atoms to the silver nanoparticles and thus reduces the oxidized silver species. Notably, the NH_3-SCO reaction over 10 wt % Ag/Al_2O_3 could be divided into three reaction regions: the light-off region (150−225 °C) where the formation of both N_2 and N_2O rapidly increased; the high-efficiency region (225−350 °C) where N_2 formation was highly efficient and N_2O formation decreased gradually; and the high-temperature region (350−450 °C) in which NO production gradually increased, accompanied by a slight decrease in N_2 formation. The reaction pathway is nearly related to the activation of oxygen on the silver nanoparticles; that is, a slow activation rate resulted in the formation of N_2O, whereas a rapid dehydrogenation of NH_3 induced the generation of NO. Instead, appropriate rates for O_2 activation and NH_3 dehydrogenation are essential for N_2 formation during NH_3 oxidation.

■ ASSOCIATED CONTENT

Supporting Information

The Supporting Information is available free of charge at https://pubs.acs.org/doi/10.1021/acscatal.1c01054.

BET surface area analysis results, XRD patterns, HR-TEM images, and DRIFTS spectra (PDF)

■ AUTHOR INFORMATION

Corresponding Author

Hong He − *State Key Joint Laboratory of Environment Simulation and Pollution Control, Research Center for Eco-Environmental Sciences, Chinese Academy of Sciences, Beijing 100085, China; Center for Excellence in Regional Atmospheric Environment, Institute of Urban Environment, Chinese Academy of Sciences, Xiamen 361021, China; University of Chinese Academy of Sciences, Beijing 100049, China*; Email: honghe@rcees.ac.cn

Authors

Guangyan Xu − *State Key Joint Laboratory of Environment Simulation and Pollution Control, Research Center for Eco-Environmental Sciences, Chinese Academy of Sciences, Beijing 100085, China*; orcid.org/0000-0002-4275-7517

Yu Zhang − *State Key Laboratory of Engine Reliability, Weifang 261061, China*

Jingguo Lin − *State Key Laboratory of Engine Reliability, Weifang 261061, China*
Yibao Wang − *State Key Laboratory of Engine Reliability, Weifang 261061, China*
Xiaoyan Shi − *State Key Joint Laboratory of Environment Simulation and Pollution Control, Research Center for Eco-Environmental Sciences, Chinese Academy of Sciences, Beijing 100085, China; Center for Excellence in Regional Atmospheric Environment, Institute of Urban Environment, Chinese Academy of Sciences, Xiamen 361021, China; University of Chinese Academy of Sciences, Beijing 100049, China*
Yunbo Yu − *State Key Joint Laboratory of Environment Simulation and Pollution Control, Research Center for Eco-Environmental Sciences, Chinese Academy of Sciences, Beijing 100085, China; Center for Excellence in Regional Atmospheric Environment, Institute of Urban Environment, Chinese Academy of Sciences, Xiamen 361021, China; University of Chinese Academy of Sciences, Beijing 100049, China;* orcid.org/0000-0003-2935-0955

Complete contact information is available at:
https://pubs.acs.org/10.1021/acscatal.1c01054

Author Contributions

The manuscript was written through the contributions of all authors. All authors have approved the final version of the manuscript.

Notes

The authors declare no competing financial interest.

■ ACKNOWLEDGMENTS

The authors acknowledge the National Key R&D Program of China (2017YFC0211101), the National Natural Science Foundation of China (21906171, 21673277, and 21637005), the Strategic Priority Research Program of the Chinese Academy of Sciences (XDA23010200), and the Science Fund of State Key Laboratory of Engine Reliability (SKLER-201802).

■ REFERENCES

(1) Chen, J. G.; Crooks, R. M.; Seefeldt, L. C.; Bren, K. L.; Bullock, R. M.; Darensbourg, M. Y.; Holland, P. L.; Hoffman, B.; Janik, M. J.; Jones, A. K.; Kanatzidis, M. G.; King, P.; Lancaster, K. M.; Lymar, S. V.; Pfromm, P.; Schneider, W. F.; Schrock, R. R. Beyond fossil fuel-driven nitrogen transformations. *Science* **2018**, *360*, No. eaar6611.
(2) Beale, A. M.; Gao, F.; Lezcano-Gonzalez, I.; Peden, C. H. F.; Szanyi, J. Recent advances in automotive catalysis for NOx emission control by small-pore microporous materials. *Chem. Soc. Rev.* **2015**, *44*, 7371−7405.
(3) Lambert, C. K. Current state of the art and future needs for automotive exhaust catalysis. *Nat. Catal.* **2019**, *2*, 554−557.
(4) Busca, G.; Pistarino, C. Abatement of ammonia and amines from waste gases: a summary. *J. Loss Prev. Process Ind.* **2003**, *16*, 157−163.
(5) Chmielarz, L.; Jabłońska, M. Advances in selective catalytic oxidation of ammonia to dinitrogen: a review. *RSC Adv.* **2015**, *5*, 43408−43431.
(6) Svintsitskiy, D. A.; Kibis, L. S.; Stadnichenko, A. I.; Slavinskaya, E. M.; Romanenko, A. V.; Fedorova, E. A.; Stonkus, O. A.; Doronkin, D. E.; Marchuk, V.; Zimina, A.; Casapu, M.; Grunwaldt, J. D.; Boronin, A. I. Insight into the nature of active species of Pt/Al_2O_3 catalysts for low temperature NH_3 oxidation. *Chemcatchem* **2020**, *12*, 867−880.
(7) Ma, H.; Schneider, W. F. Structure- and temperature-dependence of Pt-catalyzed ammonia oxidation rates and selectivities. *ACS Catal.* **2019**, *9*, 2407−2414.
(8) Lin, M.; An, B.; Niimi, N.; Jikihara, Y.; Nakayama, T.; Honma, T.; Takei, T.; Shishido, T.; Ishida, T.; Haruta, M.; Murayama, T. Role of the acid site for selective catalytic oxidation of NH_3 over Au/Nb_2O_5. *ACS Catal.* **2019**, *9*, 1753−1756.
(9) Dann, E. K.; Gibson, E. K.; Blackmore, R. H.; Catlow, C. R. A.; Collier, P.; Chutia, A.; Erden, T. E.; Hardacre, C.; Kroner, A.; Nachtegaal, M.; Raj, A.; Rogers, S. M.; Taylor, S. F. R.; Thompson, P.; Tierney, G. F.; Zeinalipour-Yazdi, C. D.; Goguet, A.; Wells, P. P. Structural selectivity of supported Pd nanoparticles for catalytic NH_3 oxidation resolved using combined operando spectroscopy. *Nat. Catal.* **2019**, *2*, 157−163.
(10) Chen, W.; Ma, Y.; Qu, Z.; Liu, Q.; Huang, W.; Hu, X.; Yan, N. Mechanism of the selective catalytic oxidation of slip ammonia over Ru-Modified Ce-Zr complexes determined by in situ diffuse reflectance infrared Fourier transform spectroscopy. *Environ. Sci. Technol.* **2014**, *48*, 12199−12205.
(11) Cui, X.; Zhou, J.; Ye, Z.; Chen, H.; Li, L.; Ruan, M.; Shi, J. Selective catalytic oxidation of ammonia to nitrogen over mesoporous CuO/RuO_2 synthesized by co-nanocasting-replication method. *J. Catal.* **2010**, *270*, 310−317.
(12) Gang, L.; Anderson, B. G.; van Grondelle, J.; van Santen, R. A.; van Gennip, W. J. H.; Niemantsverdriet, J. W.; Kooyman, P. J.; Knoester, A.; Brongersma, H. H. Alumina-supported Cu-Ag catalysts for ammonia oxidation to nitrogen at low temperature. *J. Catal.* **2002**, *206*, 60−70.
(13) Burch, R.; Southward, B. W. L. The nature of the active metal surface of catalysts for the clean combustion of biogas containing ammonia. *J. Catal.* **2001**, *198*, 286−295.
(14) Li, P.; Zhang, R.; Liu, N.; Royer, S. Efficiency of Cu and Pd substitution in Fe-based perovskites to promote N_2 formation during NH_3 selective catalytic oxidation (NH_3-SCO). *Appl. Catal., B* **2017**, *203*, 174−188.
(15) Jabłońska, M.; Palkovits, R. Copper based catalysts for the selective ammonia oxidation into nitrogen and water vapour-Recent trends and open challenges. *Appl. Catal., B* **2016**, *181*, 332−351.
(16) Lee, S. M.; Hong, S. C. Promotional effect of vanadium on the selective catalytic oxidation of NH_3 to N_2 over $Ce/V/TiO_2$ catalyst. *Appl. Catal., B* **2015**, *163*, 30−39.
(17) Chmielarz, L.; Kuśtrowski, P.; Rafalska-Łasocha, A.; Dziembaj, R. Selective oxidation of ammonia to nitrogen on transition metal containing mixed metal oxides. *Appl. Catal., B* **2005**, *58*, 235−244.
(18) Darvell, L. I.; Heiskanen, K.; Jones, J. M.; Ross, A. B.; Simell, P.; Williams, A. An investigation of alumina-supported catalysts for the selective catalytic oxidation of ammonia in biomass gasification. *Catal. Today* **2003**, *81*, 681−692.
(19) Yang, M.; Wu, C.; Zhang, C.; He, H. Selective oxidation of ammonia over copper-silver-based catalysts. *Catal. Today* **2004**, *90*, 263−267.
(20) Zhang, T.; Chang, H.; You, Y.; Shi, C.; Li, J. Excellent activity and selectivity of one-pot synthesized Cu-SSZ-13 catalyst in the selective catalytic oxidation of ammonia to nitrogen. *Environ. Sci. Technol.* **2018**, *52*, 4802−4808.
(21) Hinokuma, S.; Kiritoshi, S.; Kawabata, Y.; Araki, K.; Matsuki, S.; Sato, T.; Machida, M. Catalytic ammonia combustion properties and operando characterization of copper oxides supported on aluminum silicates and silicon oxides. *J. Catal.* **2018**, *361*, 267−277.
(22) Jabłońska, M.; Król, A.; Kukulska-Zajac, E.; Tarach, K.; Chmielarz, L.; Góra-Marek, K. Zeolite Y modified with palladium as effective catalyst for selective catalytic oxidation of ammonia to nitrogen. *J. Catal.* **2014**, *316*, 36−46.
(23) Qi, G.; Gatt, J. E.; Yang, R. T. Selective catalytic oxidation (SCO) of ammonia to nitrogen over Fe-exchanged zeolites prepared by sublimation of $FeCl_3$. *J. Catal.* **2004**, *226*, 120−128.
(24) Long, R. Q.; Yang, R. T. Superior ion-exchanged ZSM-5 catalysts for selective catalytic oxidation of ammonia to nitrogen. *Chem. Commun.* **2000**, *17*, 1651−1652.

(25) Gang, L.; Anderson, B. G.; van Grondelle, J.; van Santen, R. A. Intermediate species and reaction pathways for the oxidation of ammonia on powdered catalysts. *J. Catal.* **2001**, *199*, 107−114.
(26) Gang, L.; Anderson, B. G.; van Grondelle, J.; van Santen, R. A. Low temperature selective oxidation of ammonia to nitrogen on silver-based catalysts. *Appl. Catal., B* **2003**, *40*, 101−110.
(27) Zhang, L.; Zhang, C.; He, H. The role of silver species on Ag/Al_2O_3 catalysts for the selective catalytic oxidation of ammonia to nitrogen. *J. Catal.* **2009**, *261*, 101−109.
(28) Zhang, L.; He, H. Mechanism of selective catalytic oxidation of ammonia to nitrogen over Ag/Al_2O_3. *J. Catal.* **2009**, *268*, 18−25.
(29) Zawadzki, J. The mechanism of ammonia oxidation and certain analogous reactions. *Discuss. Faraday Soc.* **1950**, *8*, 140−152.
(30) Mieher, W. D.; Ho, W. Thermally activated oxidation of NH_3 on Pt(111) - Intermediate species and reaction mechanisms. *Surf. Sci.* **1995**, *322*, 151−167.
(31) Popa, C.; van Santen, R. A.; Jansen, A. P. J. Density-functional theory study of NHx oxidation and reverse reactions on the Rh(111) surface. *J. Phys. Chem. C* **2007**, *111*, 9839−9852.
(32) Ramis, G.; Yi, L.; Busca, G. Ammonia activation over catalysts for the selective catalytic reduction of NOx and the selective catalytic oxidation of NH_3. An FT-IR study. *Catal. Today* **1996**, *28*, 373−380.
(33) Amores, J. G.; Escribano, V. S.; Ramis, G.; Busca, G. An FT-IR study of ammonia adsorption and oxidation over anatase-supported metal oxides. *Appl. Catal., B* **1997**, *13*, 45−58.
(34) Olofsson, G.; Hinz, A.; Andersson, A. A transient response study of the selective catalytic oxidation of ammonia to nitrogen on Pt/CuO/Al_2O_3. *Chem. Eng. Sci.* **2004**, *59*, 4113−4123.
(35) Burch, R.; Southward, B. W. L. Highly selective catalysts for conversion of ammonia to nitrogen in gasified biomass. *Chem. Commun.* **1999**, *16*, 1475−1476.
(36) Burch, R.; Southward, B. W. L. A novel application of trapping catalysts for the selective low-temperature oxidation of NH_3 to N_2 in simulated biogas. *J. Catal.* **2000**, *195*, 217−226.
(37) Wang, F.; Ma, J.; He, G.; Chen, M.; Zhang, C.; He, H. Nanosize effect of Al_2O_3 in Ag/Al_2O_3 catalyst for the selective catalytic oxidation of ammonia. *ACS Catal.* **2018**, *8*, 2670−2682.
(38) Wang, F.; He, G.; Zhang, B.; Chen, M.; Chen, X.; Zhang, C.; He, H. Insights into the activation effect of H_2 pretreatment on Ag/Al_2O_3 catalyst for the selective oxidation of ammonia. *ACS Catal.* **2019**, *9*, 1437−1445.
(39) Lomachenko, K. A.; Borfecchia, E.; Negri, C.; Berlier, G.; Lamberti, C.; Beato, P.; Falsig, H.; Bordiga, S. The Cu-CHA deNOx catalyst in action: temperature-dependent NH_3-assisted selective catalytic reduction monitored by operando XAS and XES. *J. Am. Chem. Soc.* **2016**, *138*, 12025−12028.
(40) Xu, G.; Ma, J.; Wang, L.; Lv, Z.; Wang, S.; Yu, Y.; He, H. Mechanism of the H_2 effect on NH_3-selective catalytic reduction over Ag/Al_2O_3: Kinetic and diffuse reflectance infrared Fourier transform spectroscopy studies. *ACS Catal.* **2019**, *9*, 10489−10498.
(41) Xu, G.; Ma, J.; Wang, L.; Xie, W.; Liu, J.; Yu, Y.; He, H. Insight into the origin of sulfur tolerance of Ag/Al_2O_3 in the H_2-C_3H_6-SCR of NOx. *Appl. Catal., B* **2019**, *244*, 909−918.
(42) Xu, G.; Ma, J.; He, G.; Yu, Y.; He, H. An alumina-supported silver catalyst with high water tolerance for H_2 assisted C_3H_6-SCR of NOx. *Appl. Catal., B* **2017**, *207*, 60−71.
(43) Xu, G.; Yu, Y.; He, H. Silver valence state determines the water tolerance of Ag/Al_2O_3 for the H_2-C_3H_6-SCR of NOx. *J. Phys. Chem. C* **2018**, *122*, 670−680.
(44) Seyedmonir, S.; Strohmayer, D. E.; Geoffroy, G. L.; Vannice, M. A.; Young, H. W.; Linowski, J. W. Characterization of supported silver catalysts: I. Adsorption of O_2, H_2, N_2O, and the H_2-titration of adsorbed oxygen on well-dispersed Ag on TiO_2. *J. Catal.* **1984**, *87*, 424−436.
(45) Xu, G.; Wang, H.; Yu, Y.; He, H. Role of silver species in H_2-NH_3-SCR of NOx over Ag/Al_2O_3 catalysts: Operando spectroscopy and DFT calculations. *J. Catal.* **2021**, *395*, 1−9.
(46) Shibata, J.; Shimizu, K.-i.; Takada, Y.; Shichi, A.; Yoshida, H.; Satokawa, S.; Satsuma, A.; Hattori, T. Structure of active Ag clusters in Ag zeolites for SCR of NO by propane in the presence of hydrogen. *J. Catal.* **2004**, *227*, 367−374.
(47) Kim, P. S.; Kim, M. K.; Cho, B. K.; Nam, I.-S.; Oh, S. H. Effect of H_2 on deNOx performance of HC-SCR over Ag/Al_2O3: Morphological, chemical, and kinetic changes. *J. Catal.* **2013**, *301*, 65−76.
(48) Kannisto, H.; Skoglundh, M.; Arve, K.; Olsson, E.; Härelind, H. Direct observation of atomically-resolved silver species on a silver alumina catalyst active for selective catalytic reduction of nitrogen oxides. *Catal. Sci. Technol.* **2019**, *9*, 6213−6216.
(49) Cant, N. W.; Little, L. H. Lewis and Brønsted acid sites on silica-alumina. *Nature* **1966**, *211*, 69−70.
(50) Hu, C.; Peng, T.; Hu, X.; Nie, Y.; Zhou, X.; Qu, J.; He, H. Plasmon-Induced Photodegradation of Toxic Pollutants with Ag-AgI/Al_2O_3 under Visible-Light Irradiation. *J. Am. Chem. Soc.* **2010**, *132*, 857−862.

https://doi.org/10.1021/acscatal.1c01054
ACS Catal. 2021, 11, 5506−5516